
Universitat
de les Illes Balears

# PATTERN FORMATION IN CLONAL PLANTS

**submitted by**
FRANCESCA SCHÖNSBERG

**MASTER'S THESIS**
Master's degree in Physics of Complex Systems
at the
UNIVERSITAT DE LES ILLES BALEARS

**Academic year:** 2015-2016

**Date of submission of the Master's thesis:** September 22, 2016

**Supervisor:** Prof. Dr. Damià Gomila, Instituto de Fsica Interdisciplinar y Sistemas Complejos IFISC (CSIC-UIB)

**Co-Supervisor:** Prof. Dr. Emilio Hernández-García, Instituto de Fsica Interdisciplinar y Sistemas Complejos IFISC (CSIC-UIB)

# Contents


**1 Introduction** **6**

1.1 Current state of the field . . . . . 7

1.2 Description of the model . . . . . 8

**2 Analytical Study** **12**

2.1 Linar stability analisis of the homogeneous system . . . . . 12

2.2 Linear stability analysis of the spatial system . . . . . 13

2.2.1 Positive branch . . . . . 14

2.2.2 Negative branch . . . . . 15

2.2.3 Singularity of the model . . . . . 17

2.3 Linear stability analysis of the spatial system adding a diffusion . . . . . 19

**3 Numerical validation** **21**

3.1 Confirming the effect of $\delta|\nabla n(x,y,t)|^2$ . . . . . 21

3.1.1 Exploring the dependence of $\delta$ with the velocity of expansion. . . . . 22

3.1.2 Growth dynamics with random initial condition lacking of radial symmetry . . 23

3.2 Bifurcation diagram including stability regions of patterns . . . . . 24

**4 Re-population strategies** **25**

**5 Discussion** **26**

**6 Appendix A: Further studies on the model in Sec. 2.3** **28**

6.1 A.1: Analytical solutions of the model . . . . . 28

6.2 A.2: Phase diagram with different parameters . . . . . 29

**7 Appendix B: Influence of the parameters $a$, $\omega$ and $\alpha$ on the growth velocity** **31**

## Abstract

The precise dynamical features emerging from meadows of seagrasses (marine clonal plants) are not well understood. Research on modeling clonal plants tries to define the relative contribution of the different natural components on the global development of a meadow as well as on its extinction. To this day, no model is providing a simple, analytically tractable, comprehensive description of the dynamical features emerging from seagrasses.

In the following thesis we approach this gap, inspired by the numerical results of a recent model ($ABD$ model) (Ruiz et al., 2016). Specifically, starting from the numerical bifurcation and phase diagrams of the $ABD$ model we build a single partial differential equation reproducing the behavior. In particular, we expose the analytical and numerical arguments verifying the compatibility of the two models. Overall, we show that the complex dynamical behavior emerging in the growth of seagrass meadows can be reduced to a single equation, thus providing a possible predictive tool for designing effective re-population strategies and prevent extinctions.

# 1 Introduction

The balance of marine ecosystems is relevantly based on seagrasses, which constitute one of the most productive biomes on the earth (Duarte and Chiscano, 1999). Seagrasses are essential trophic factors for the surrounding ecosystems (Duarte, 2002). Further, they are responsible for about 15% of carbon storage in the ocean (Duarte and Chiscano, 1999). Such storages, created in the soil underneath them and lasting up to millennias (Fourqurean et al., 2012), make seagrasses essential factors to prevent and limit greenhouse emissions (such as $CO_2$) thus mitigating climate change (Mcleod et al., 2011).
Seagrasses are clonal plants, rather new plants (clones) originates from parts of another plant without the production of seeds or spores. In optimal conditions, seagrasses have shoots living up to 50 years and clones lasting for millenias. Accordingly, their growth and colonization is very slow. On the other side, they are highly vulnerable to disturbances which increment their mortality, causing rapid losses in the vegetation (Jordà et al., 2012).
The Mediterranean seagrass *Posidonia Oceanica*, for example, has been experiencing a fast decay in the last 50 years mainly due to local anthropogenic factors transforming the coastal zones (Marbà et al., 2014). Furthermore, the increment of seawater temperatures, which is progressing due to climate warming, has been pointed as an additional key factor causing the extinction of *Posidonia* (Jordà et al., 2012).
Therefore, if, on one side, seagrasses provide the Mediterranean carbon sink, on the other side they are highly affected by the results of greenhouse gases increment, as global warming. Such negative loop is clearly unsustainable, given the additional anthropogenic factors which are keeping contributing to global warming (animal based alimentation, industry, etc.) and to the loss of *Posidonia* (coastal and cruise tourism, water pollution, etc), and will lead to catastrophic consequences if no action are rapidly taken to unbalance it.
Attempting the effective conservation of seagrasses needs therefore to be sinergistically addressed with different methods and from different areas. A contribution can derive from the development of quantitative models capable of predicting the responses of seagrasses to disturbances (Duarte, 2002) and usable to design effective re-population strategies.
In the following thesis we focus on this last point. To this day, numerical models have been designed and showed to successfully reproduce the dynamical features of clonal plants growth (Ruiz et al., 2016). However, they are limited by being highly complex, thus analyzable only through large numerical simulations. In this thesis we propose a single partial differential equation which reproduces the dynamical features of clonal plants, thus providing a simple, analytically tractable tool describing their behavior.
In the next sections we will define the current state of the field in modeling clonal plants growth and introduce our work.

## 1.1 Current state of the field

Modeling the growth of rhizomatous (clonal) plants, such as *Posidonia*, have been a matter of studies since the 90$s$. In this context, an amount of scientific work have been devoted to approximate their space occupation, from simple random-walk processes (Routledge, 1990) to the definition of growth rules explaining the non-linearity of clonal growth (Sintes et al., 2005). This latter work defined the three key components in seagrasses development:

- **the extension rate of the rhizome:** The rhizome of a plant, whose initial part is defined as apex, grows horizontally on the seabed.
- **the distance between shoots**: When the apex moves it leaves behind new shoots at a characteristic distance. Each of these shoots have a lifetime influenced by external disturbances.
- **the branching rate and the branching angle**: The apex can separate in two branches. Each rhizome is thus characterized by a branching rate and a branching angle.

In Fig. 1 we report a sketch of what was explained above.

The model derived from these assumptions reproduced accurately the growth of a single plant but

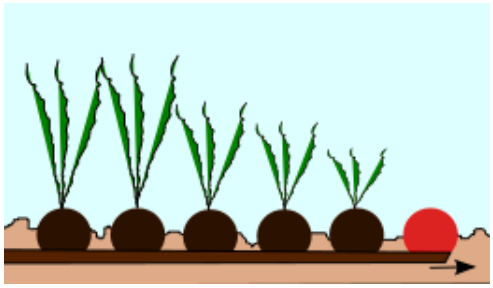

**Figure 1:** In this picture we sketch the key components of the growth of seagrasses as described in the text. The brown circles represent shoots and the red circle the apex of the rhizome growing on the x axes. In this schematic branching is not presented. The proportions in the picture are unrealistic and emphasize the key components.

was unable to catch the properties emerging when plants interacts, such as pattern formation.

In order to fill such gap a recent work (Ruiz et al., 2016) proposed a coarse grained approximation (the $ABD$ model) describing the evolution of the spatial density of apices $n_a(\overrightarrow{r},\phi,t)$ and shoots $n_s(\overrightarrow{r},t)$, where $\overrightarrow{r}=(x,y)$ and $\phi$ is the angle of growth. In particular they defined the following set of equations:

$$
\begin{aligned}
&1.\quad n_t(\overrightarrow{r},t) = n_s(\overrightarrow{r},t) + \int_0^{2\pi} n_a(\overrightarrow{r},\phi,t)d\phi \\
&2.\quad \partial_t n_a(\overrightarrow{r},\phi,t) = -\omega_d(n_t)n_a(\overrightarrow{r},\phi,t) - \overrightarrow{v}\cdot\nabla n_a(\overrightarrow{r},\phi,t) + \frac{\omega_b}{2}[n_a(\overrightarrow{r},\phi+\phi_b,t) + n_a(\overrightarrow{r},\phi-\phi_b,t)] \\
&3.\quad \partial_t n_s(\overrightarrow{r},t) = -\omega_d(n_t)n_s(\overrightarrow{r},t) + \frac{v}{\rho}\int_0^{2\pi} n_a(\overrightarrow{r},\phi,t)d\phi \\
&4.\quad \omega_d(n_t) = \omega_{d0} + \int\int \mathcal{K}(\overrightarrow{r}-\overrightarrow{r}')(1-e^{-an_t(\overrightarrow{r}')})d\overrightarrow{r}' + bn_t^2 \\
&5.\quad \mathcal{K}(\overrightarrow{r}) = \kappa\mathcal{G}(\sigma_\kappa,\overrightarrow{r}) - \omega_{d0}\mathcal{G}(\sigma_0,\overrightarrow{r})
\end{aligned}
\tag{1}
$$

where $n_t$ is the total number of shoots, the velocity vector is $\overrightarrow{v}=v(\cos\phi,\sin\phi)$ with $v$ constant, the subscript $d$ stands for *death* and the subscript $b$ for *birth* (e.g.: $w_d(n_t) = death\ rate\ of\ total\ shoots$). Rather the parameters of the model are $v,\rho,\omega_b,\omega_{d0},\kappa$ and the rest are variables. Generally:

- the first Eq. models the total density of shoots given by the sum of shoots and apices growing in every direction.
- The second Eq. models the evolution of the density of apices, composed by the intrinsic mortality, a drift in the direction of the elongation (advection term) and by the branching process.
- The third Eq. models the evolution of the density of shoots, accounting the shoots left behind from the apices.
- The fourth Eq. defines the dependency of the death rate of shoots on the intrinsic mortality and on the total density, in particular on the non local interactions (integral) and a local saturation ($bn_t^2$).
- Finally Eq. 5 corresponds to the kernel which weights the interaction of the shoot at position $\overrightarrow{r'}$ with those in the neighborhood, it corresponds to a double Gaussian giving rise to a Mexican hat shape, promoting cooperation at short ranges and competition at large ranges.

The model led to successful results allowing to understand qualitatively the non-linear behavior of the meadows, furthermore it reproduced a variety of spatial patterns accurately comparable with real density measurements.
(Ruiz et al., 2016) studied systematically the complex spatial patterns and found the bifurcation and phase diagrams numerically.
However, despite the success in reproducing real data, the model present some limitations. In particular, the analytical predictions and the computational speed are highly limited, as the model is composed at least by nine two-dimensional fields, 1 for the shoots and the rest for the apices. Indeed, the angle $\phi$ is discretized for computational reasons, and the minimal number of directions that the author found to be necessary to separate is 8.
Starting from the results of the $ABD$ model and the set of equations that defines it we propose a single $2D$ partial differential equation describing the global evolution of the total density.
In the following section we present how we inferred the equation from the results of the numerical simulations. We then show, through analytical and numerical studies, that it fully reproduces the dynamical features of the $ABD$ model (Ruiz et al., 2016), thus providing an analytically tractable tool describing seagrasses growth. Finally we use this new equation to propose a design for re-population strategies.

## 1.2 Description of the model

In this section we describe how we derived the equation for the total density of seagrasses. For this purpose we will assume the results of the $ABD$ model (Ruiz et al., 2016). In particular we try to reproduce that:

- In the absence of interactions the velocity at which the populated solution invades the unpopulated one is mainly dominated by the velocity of the rhizome (apices) growth, in a direction perpendicular to the interface between the populated and unpopulated areas. We call this interface as *front*.
- Considering the mortality rate as the control parameter, the homogeneous unpopulated solution undergoes a transcritical bifurcation to a populated solution. This bifurcation, can be subcritical

or supercritical depending on the parameters. One of the branches of the transcritical bifurcation ends in a saddle node.

- Considering the mortality rate as the control parameter, the homogeneous populated solution undergoes a Turing bifurcation (also called modulational instability (MI) point). Such bifurcation corresponds to the destabilization of the homogeneous solution to form spatial patterns for perturbations of a certain wave length dependent on the parameters of the system.

**Mortality and Interactions.** As introduced in the previous sections the mortality characterizing the evolution of the density of shoots depends on

- The intrinsic mortality of a shoot (defined $\omega_{d0}$ in (Ruiz et al., 2016) and here simply $\omega$);
- A local saturation term $bn^2$ which ensures the physical limitation of growth, where $b$ relates to the carrying capacity determining the maximum density of the populated state;
- The non local interactions of each shoot with the neighboring ones.

Overall, the total mortality rate can thus be written as:

$$\omega_{tot}(n) = \omega_{death} - \omega_{birth} = \omega + I(n(\overrightarrow{r}, t)) + bn^2 \tag{2}$$

where $I(n(\overrightarrow{r}, t))$ is the function defining the weight of the neighbors of the spot $n(\overrightarrow{r}, t)$ with $\overrightarrow{r} = (x, y)$.
The shoots interact by competition/cooperation at long/short distances, thus we define, as in (Ruiz et al., 2016):

$$I(n(\overrightarrow{r}, t)) = \int\int \mathcal{K}(\overrightarrow{r} - \overrightarrow{r}')n(\overrightarrow{r}', t)d\overrightarrow{r}' \tag{3}$$

where $\mathcal{K}$ is a cooperative-competitive (mexican hat) symmetric kernel, formed by two Gaussian. In (Ruiz et al., 2016) the authors multiply the kernel by $(1 - e^{-an(\overrightarrow{r}')})$ in order to ensure the positivity of $\omega_{tot}$, which else would not quantify the death of plants but the birth. In our case we do not care as $\omega_{tot}$ includes the death and the birth, given that we do not explicitly model the branching (see next paragraph).
Eq. (3), can be expanded and simplified, as suggested in (Murray, 2002). We will perform here the expansion for the one-dimensional case to show the underlying idea in a simple way, then, we remand to the book for the generalization in two dimensions.
Considering a one dimensional system, we can re-write Eq. (3) as:

$$I(n(x, t)) = \int \mathcal{K}(x - x')n(x', t)dx' \tag{4}$$

Then we substitute $s = x - x'$, obtaining:

$$I(n(x - s, t)) = \int \mathcal{K}(s)n(x - s, t)ds \tag{5}$$

Considering that $s$ is quite small we can Taylor expand $n(x-s)$ about $x$, obtaining:

$$\int \mathcal{K}(s)n(x-s,t)ds = \int \mathcal{K}(s)\Big[n(x,t) - s\frac{\partial n(x,t)}{\partial x} + \frac{s^2}{2}\frac{\partial^2 n(x,t)}{\partial x^2} - \frac{s^3}{3!}\frac{\partial^3 n(x,t)}{\partial x^3} + \\ + \frac{s^4}{4!}\frac{\partial^4 n(x,t)}{\partial x^4} - ...\Big]ds \tag{6}$$

Given that $\mathcal{K}$ is symmetric, the integral of all odd powers will go to zero, then, defining the moments of the kernel as:

$$\kappa_{2\kappa'} = \frac{1}{2\kappa'!}\int s^{2\kappa'}\mathcal{K}(s)ds, \quad \text{with} \quad \kappa' = 0, 1, 2.. \tag{7}$$

permits us to simplify the original equation as:

$$I(n) = \kappa_0 n + \kappa_2\frac{\partial^2 n}{\partial x^2} + \kappa_4\frac{\partial^4 n}{\partial x^4} + ... \tag{8}$$

where we neglect higher moments as the kernel get smaller and smaller.
The expansion and approximations done so far can be generalized to two dimensions (Murray, 2002), yielding to a result of the same form as Eq. (8), namely in $2D$:

$$I(n) = \rho_0 n + \rho_2(\nabla^2 n) + \rho_4(\nabla^4 n) + .. \tag{9}$$

Therefore the evolution of the density $n$, whose mortality is modulated by the interactions evolves as:

$$\partial_t n = -\omega_{tot}(n)n = -\omega n - \rho_0 n^2 - bn^3 - \rho_2(\nabla^2 n)n - \rho_4(\nabla^4 n)n \tag{10}$$

Such equation, excluding the spatial terms, gives rise to a transcritical bifurcation and a saddle node, as we study in Sec 2.1.

**Evolution of the apices** The results in (Ruiz et al., 2016) lead to infer that the main contribution given by the 8 fields describing the growth and branching of the apices is the constant expansion of the populated solution at the velocity of growth of the rhizome, in a direction perpendicular to the front.
We modeled such behavior introducing a drift. Namely, considering a 1-dimensional case, we define the evolution of the density as:

$$\partial_t n(x,t) = \nu\partial_x n(x,t) + f(n(x,t)) \tag{11}$$

where $\nu\partial_x n(x,t)$ is the drift, characterizing the movement at a constant velocity $\nu$, and $f(n)$ represents a function modifying the shape of the front.
Focusing only on the drift we notice that it can not correctly reproduce the results such that. Indeed, as visible in Fig. 2, the derivative at the position of the front ($x_f$ in the one dimensional example shown in the picture) can be negative (picture on the right) or positive depending on the shape. This would make the front moving to the left when the derivative is positive as well as when it is negative. This second case would be wrong, as we assume from the results in (Ruiz et al., 2016) that the populated solution grows over the unpopulated and never vice-versa. We solve this problem by approximating

$$\nu \approx \nu'\frac{\nabla n(x_0)}{|\nabla n(x_0)|} \tag{12}$$

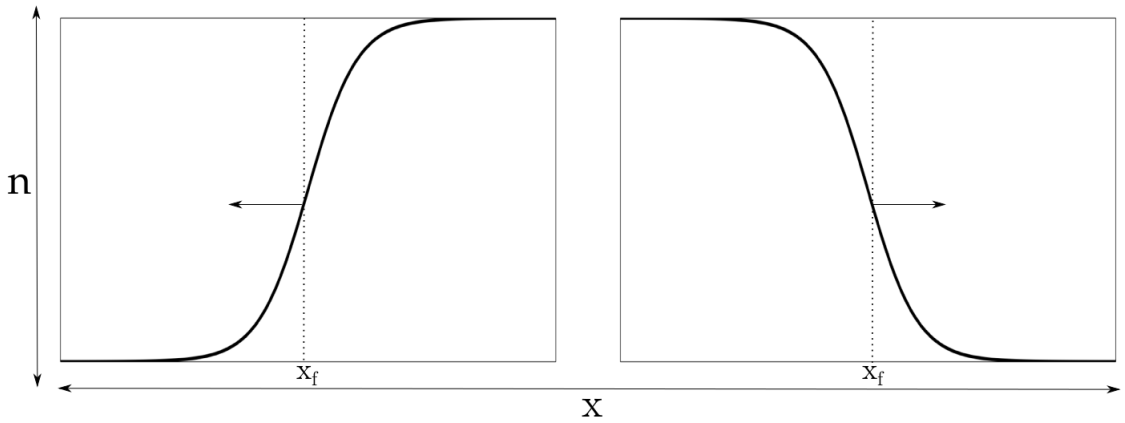


**Figure 2:** Schematic of a potential cut in the $y$ plane, showing the front between homogeneous populated solution and unpopulated one. The arrow depict the growth direction of the front.

where $x_0$ represent a general point at which we evaluate the derivative. In this way the velocity is given by $\nu'$ whereas $\frac{\nabla n(x_0)}{|\nabla n(x_0)|}$ gives the sign of the derivatives. Thus the drift will always go in the wanted direction as $\nabla n \cdot \nabla n = |\nabla n|^2 > 0$. Finally, to avoid difficulties in the analytical study we further approximate

$$\nu' \frac{\nabla n(x_0)}{|\nabla n(x_0)|} \approx \delta \nabla n(x_0) \tag{13}$$

where we considered the modulus as constant and incorporate it in $\delta$.
Overall, we can re-write Eq. (11) as:

$$\partial_t n(x,t) = \delta |\nabla n(x,t)|^2 + f(n(x,t)) \tag{14}$$

The same process exposed here can be generalized to two-dimensions (Gomila, 2003).
In Sec. 3 we verify that the approximations we took are correct, and the term reproduce the expected behavior.

Thus, joining the results of this and the previous paragraph, yields:

$$\partial_t n = -\omega n - \rho_0 n^2 - b n^3 - \delta |\nabla n|^2 - \rho_2 (\nabla^2 n) n - \rho_4 (\nabla^4 n) n \tag{15}$$

Now, for simplicity of visualization we set $\rho_0 \equiv -a$, $\rho_2 \equiv -\alpha$, $\rho_4 \equiv -\beta$, obtaining:

$$\partial_t n = -\omega n + a n^2 - b n^3 + \delta |\nabla n|^2 + \alpha (\nabla^2 n) n + \beta (\nabla^4 n) n \tag{16}$$

To complete the equation we add a term $\gamma(\nabla^2 n)^2$. Indeed as the higher order of (16) is $n^2$, we need to include all possible terms in the same order as they could appear in the systematical expansion of the equation, yielding:

$$\partial_t n = -\omega n + a n^2 - b n^3 + \delta |\nabla n|^2 + \alpha (\nabla^2 n) n + \beta (\nabla^4 n) n + \gamma (\nabla^2 n)^2 \tag{17}$$

This term does not influence the linear stability analysis and we are not aware of a potential analogous in the model of (Ruiz et al., 2016), therefore we write it here for completeness but we will neglect it further on.

In the following sections (Sec. 2.1 and 2.2) we perform the analytical study of Equation (16). The results, lead to the conclusion that Eq. (16) do not fully reproduce the behavior of the $ABD$ model, therefore, as we explain in Sec. 2.2.3, we introduced an additional term to Eq. (16) thus formulating an equation that, as studied in Sec. 2.3, reproduces exactly the features of the $ABD$ model.

# 2 Analytical Study

In this sections we perform the analytical analysis of the equation

$$\partial_t n(x,y,t) = -\omega n(x,y,t) + a n(x,y,t)^2 - b n(x,y,t)^3 + \delta|\nabla n(x,y,t)|^2 + \alpha(\nabla^2 n(x,y,t))n(x,y,t) + \\ +\beta(\nabla^4 n(x,y,t))n(x,y,t) + \gamma(\nabla^2 n(x,y,t))^2 \tag{18}$$

described in the previous sections. For this purpose we consider the density $n(x,y,t) \subset \mathbb{R}$ even though the physical interpretation will concern only $n(x,y,t) \subset \mathbb{R}^+$.
To simplify the analysis we set $b = 1$ and $\gamma = 0$, for the reason explained in the introduction, further from now on we call $n \equiv n(x,y,t)$, yielding:

$$\partial_t n = -\omega n + a n^2 - n^3 + \delta|\nabla n|^2 + \alpha(\nabla^2 n)n + \beta(\nabla^4 n)n \tag{19}$$

## 2.1 Linar stability analisis of the homogeneous system

Initially we consider the homogeneous system

$$\partial_t n = -\omega n + a n^2 - n^3 \tag{20}$$

and obtain the fixed points when $\partial_t n = 0$, as follows:

$$0 = -wn + an^2 - n^3 = n(-n^2 + an - w) \rightarrow \begin{cases} n_0^* = 0 \\ n_+^* = \frac{a+\sqrt{a^2-4\omega}}{2} \\ n_-^* = \frac{a-\sqrt{a^2-4\omega}}{2} \end{cases} \tag{21}$$

We see that $n_+^*$ and $n_-^*$ emerges from a saddle node bifurcation at $a^2 - 4\omega = 0$, rather $n_+^*$ and $n_-^*$ exist when $\omega < \frac{a^2}{4}$. We compute the eigenvalue

$$\lambda = -\omega + 2an^* - 3n^{*2} \tag{22}$$

in order to study the stability of each fixed point. In the case $n_0^* = 0$ the eigenvalue is $\lambda = -\omega$, it follows that when $\omega > 0$ the growth rate of the perturbation is negative, thus $n_0^*$ is stable. On the other side if $\omega < 0$ the growth rate is positive and $n_0^*$ unstable.
In the case of $n_{+/-}^* = \frac{a \pm \sqrt{a^2-4\omega}}{2}$ we obtain the corresponding eigenvalues

$$\begin{aligned} \lambda_+ &= \frac{+4\omega - a^2 - a\sqrt{a^2-4\omega}}{2} \\ \lambda_- &= \frac{+4\omega - a^2 + a\sqrt{a^2-4\omega}}{2} \end{aligned} \tag{23}$$

To facilitate the analysis we define the variable $S \equiv a^2 - 4\omega$, where $S > 0$ as condition of existence of the fixed points, thus we obtain:

$$\begin{aligned} \lambda_+ &= \frac{-S - a\sqrt{S}}{2} \\ \lambda_- &= \frac{-S + a\sqrt{S}}{2} \end{aligned} \tag{24}$$

We see that $a$ determines the stability of the branches. When $a > 0$, $\lambda_+$ is always negative instead $\lambda_-$ is negative only when $a < \sqrt{a^2 - 4\omega} \rightarrow \omega < 0$, thus $n^*_+$ is always stable and $n^*_-$ is stable when $\omega < 0$. The stability of the branches switches if $a < 0$.The results derived in this section are depicted in Fig. 3.

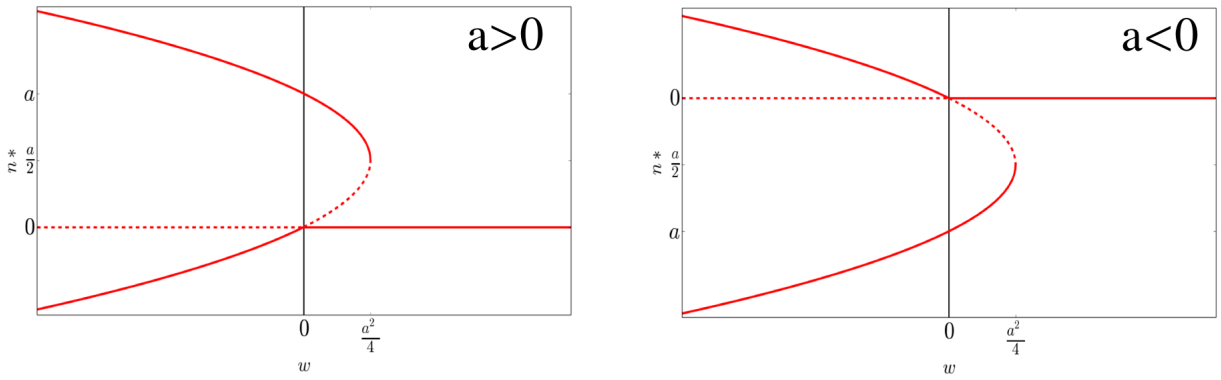


**Figure 3:** The plots represent the bifurcation diagram of the homogeneous solutions for $a > 0$ (left, subcritical) and $a < 0$ (right, supercritical). As labeled and explained in the text the saddle node emerges at $(w, n^*)=(\frac{a^2}{4}, \frac{a}{2})$. Parameters: $a = \pm 2$

## 2.2 Linear stability analysis of the spatial system

In this section we develop the linear stability analysis of the full equation (Eq. (19)). We add a small perturbation $\delta n \ll 1$ to the fixed point

$$n^* = n^* + \delta n \tag{25}$$

and study the growth rate, as follows:

$$\partial_t(\cancel{n^*} + \delta n) = -\omega(n^* + \delta n) + a(n^* + \delta n)^2 - (n^* + \delta n)^3 + \delta|\nabla(\cancel{n^*} + \delta n)|^2 + \alpha(\nabla^2(\cancel{n^*} + \delta n))(n^* + \delta n) + \\ +\beta(\nabla^4(\cancel{n^*} + \delta n))(n^* + \delta n) \tag{26}$$

where we cancel the derivatives of $n^*$ as it is a constant. We develop the terms maintaining up to $\mathcal{O}(\delta n)$, as follows:

$$\partial_t(\delta n) = \cancel{-\omega n^*} - \omega\delta n + \cancel{a n^{*2}} + 2an^*\delta n - \cancel{n^{*3}} - 3n^{*2}\delta n + \cancel{\delta(\partial_x\delta n + \partial_y\delta n)^2} + \alpha(\nabla^2\delta n)(n^*) + \\ +\beta(\nabla^4\delta n)(n^*) \tag{27}$$

where we set $-\omega n^* + a n^{*2} - n^{*3} = 0$ by definition of fixed point and the term multiplied by $\delta$ as being of order $\mathcal{O}(\delta n^2)$.

We transform the field in Fourier space, namely $\mathcal{F}(\delta n(x, y, t)) = \hat{\delta n}(q_x, q_y, t)$, such that $\mathcal{F}(\nabla^2\delta n) =$

$-q^2\hat{\delta n}$ and $\mathcal{F}(\nabla^4\delta n) = q^4\hat{\delta n}$ where $q$ represents the wavenumber, obtaining:

$$\partial_t(\hat{\delta n}) = \hat{\delta n}(-\omega + 2an^* - 3n^{*2} - \alpha q^2 n^* + \beta q^4 n^*) \tag{28}$$

Thus we study the growth rate

$$\lambda = -\omega + 2an^* - 3n^{*2} - \alpha q^2 n^* + \beta q^4 n^* \tag{29}$$

to obtain the dispersion relation (growth rate) as a function of $q$ and $\omega$ for the different fixed points. Firstly we set $\beta < 0$, such that $\lim_{q\to\infty} \lambda = -\infty$, else the system would diverge to $+\infty$ for large $q$. Then we evaluate the first derivative to find the maxima and minima of $\lambda$, yielding:

$$\frac{\partial\lambda}{\partial q} = -2\alpha q n^* + 4\beta q^3 n^* = 2qn^*(-\alpha + 2\beta q^2) = 0 \rightarrow \begin{cases} q_c = 0 \\ q_c = \pm\sqrt{\frac{\alpha}{2\beta}} \end{cases} \tag{30}$$

In the case $\alpha < 0$ the growth rate has two maxima at $q_c = \pm\sqrt{\frac{\alpha}{2\beta}}$, which corresponds to the wavenumber which will have higher growth rate ($Re[\lambda]$) thus that will grow faster forming a pattern. Instead in the case of $\alpha > 0$ the system will have only one maximum at $q_c = 0$ corresponding to the homogeneous solution analyzed in the previous section.
Therefore, as we are interested in studying the emergence of patterns, we limit $\beta < 0$ and $\alpha < 0$.
Then, we substitute the positive $q_c$ value (the maximum of the growth rate to Eq. (29)), obtaining:

$$\lambda_c = -\omega + 2an^* - 3n^{*2} - \frac{\alpha^2}{4\beta} n^* \tag{31}$$

In order to study the critical $\omega_c$ values which set the passage from $\lambda$ negative (stable fixed point) to positive (pattern formation with $q_c$ as the fastest growing wavenumber) we substitute each fixed point $n^*$ individually.

### 2.2.1 Positive branch

Firstly we substitute the positive branch of the saddle node $n^*_+ = \frac{a+\sqrt{a^2-4\omega}}{2}$ and study when $\lambda_c = 0$, as follows:

$$\lambda_c^+ = \frac{+4\omega - a^2 - a\sqrt{a^2-4\omega}}{2} - \frac{\alpha^2}{8\beta}(a + \sqrt{a^2-4\omega}) = 0 \tag{32}$$

by simply rearranging the terms we get to

$$\Big(a + \frac{\alpha^2}{4\beta}\Big)\sqrt{a^2-4\omega} = 4\omega - a\Big(a + \frac{\alpha^2}{4\beta}\Big) \tag{33}$$

For simplicity we define the variable $A \equiv \Big(a + \frac{\alpha^2}{4\beta}\Big)$, yielding:

$$A\sqrt{a^2-4\omega} = 4\omega - aA \tag{34}$$

we square both sides to eliminate the root, obtaining:

$$\begin{aligned} A^2(a^2-4\omega) &= 16\omega^2 + a^2A^2 - 8aA\omega \\ 16\omega^2 + 4A\omega(A-2a) &= 0 \end{aligned} \tag{35}$$

Thus we get:

$$4\omega(4\omega + A(A-2a)) = 0 \rightarrow \begin{cases} \omega_1 = 0 \\ \omega_2 = \frac{2aA-A^2}{4} = \frac{2a\left(a+\frac{\alpha^2}{4\beta}\right)-\left(a+\frac{\alpha^2}{4\beta}\right)^2}{4} = \frac{a^2-\left(\frac{\alpha^2}{4\beta}\right)^2}{4} \end{cases} \tag{36}$$

As we squared a radical equation we may have generated artificial results, therefore we check by direct substitution in (34) the existence of the solutions. Substituting $\omega_1 = 0$ we get:

$$A\sqrt{a^2} = -aA \rightarrow A|a| = -aA \rightarrow |a| = -a \tag{37}$$

verifying that $\omega_1$ exist only if $a < 0$.
Instead, substituting $\omega_2 = \frac{2aA-A^2}{4}$ we get:

$$\begin{aligned} A\sqrt{a^2-2aA+A^2} &= 2aA - A^2 - aA \\ \sqrt{(a-A)^2} = a - A &\rightarrow |a-A| = a - A \end{aligned} \tag{38}$$

Thus we see that $\omega_2$ exist if

$$a - A > 0 \rightarrow a - a - \frac{\alpha^2}{4\beta} > 0 \rightarrow -\frac{\alpha^2}{4\beta} > 0 \tag{39}$$

which is always true given the condition already set $\beta < 0$. In particular, given the last equality defining $\omega_2$ in (36), we see that $\omega_2 < 0$ if $a^2 - \left(\frac{\alpha^2}{4\beta}\right)^2 < 0$ $\left(\text{ rather } |a| < \left|\frac{\alpha^2}{4\beta}\right|\right)$. In the case of $a > 0$ $w_2$ can be major or minor than zero. Instead in the case of $a < 0$ we can only consider $w_2 < 0$, otherwise the fixed point is negative and the linear stability analysis as done so far wouldn't make sense (for example it would require $\beta > 0$ to impede the divergence at $q \to \infty$).

### 2.2.2 Negative branch

Then we substitute the negative branch of the saddle node $n^*_- = \frac{a-\sqrt{a^2-4\omega}}{2}$ and study when $\lambda_c = 0$, as follows:

$$\lambda_c^- = \frac{+4\omega - a^2 + a\sqrt{a^2-4\omega}}{2} - \frac{\alpha^2}{8\beta}(a - \sqrt{a^2-4\omega}) = 0 \tag{40}$$

Performing the same substitution as before, rather $A \equiv \left(a + \frac{\alpha^2}{4\beta}\right)$, it yields:

$$A\sqrt{a^2-4\omega} = -4\omega + aA \tag{41}$$

Squaring both sides yields to the same results derived in (36), as the difference in the signs cancels out. However the existence of the solutions is reversed compared to the positive branch:
Substituting $\omega_1 = 0$ to (41) we get:

$$A|a| = a|A| \rightarrow |a| = a \tag{42}$$

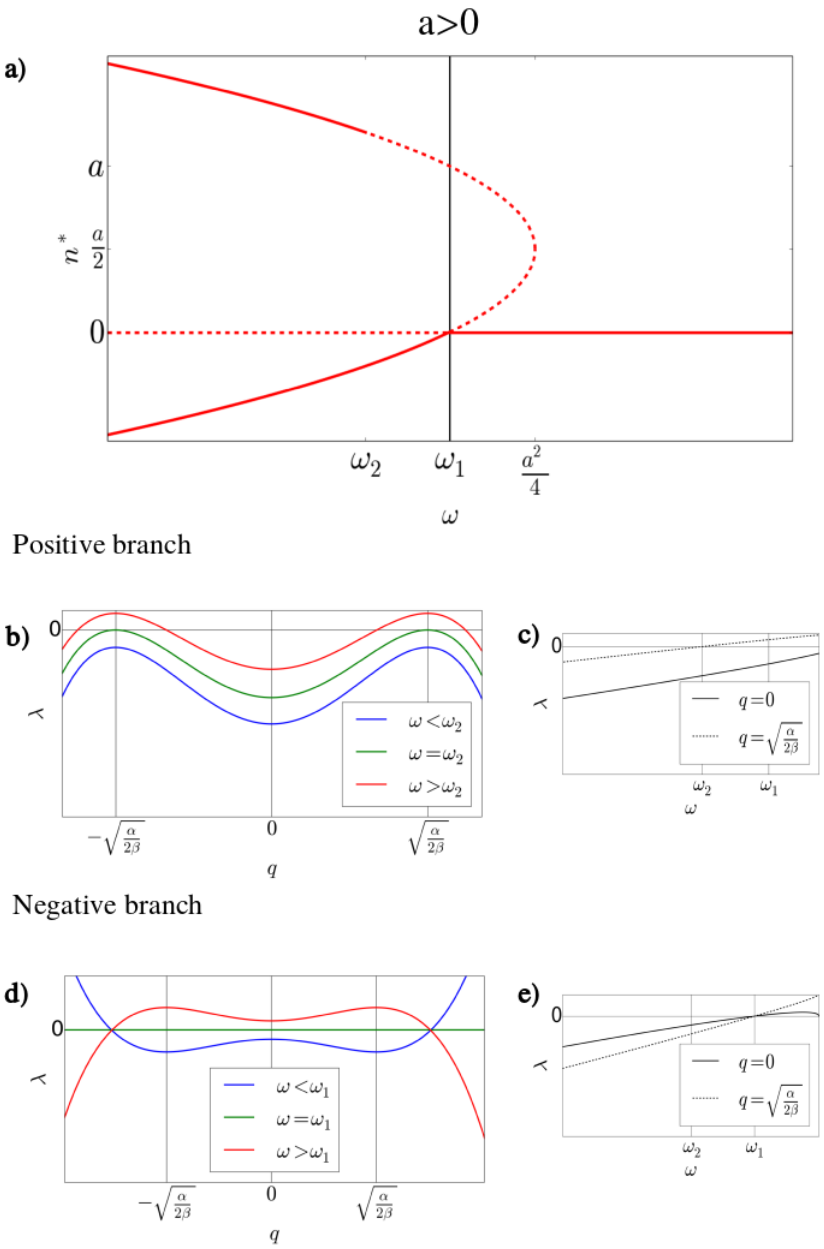


**Figure 4:** The plots sketch the results derived in this section for $a > 0$. a) Represents the bifurcation diagram when introducing the modulation instability point. b) and d) represent the growth rate for different values of $\omega$, as labeled for the positive and negative branches ($n^*_+$ and $n^*_-$). c) and e) represent the growth rate as a function function of $\omega$ for the critical wave numbers. As explained in the text the blue line of d) change the sign ($\lim_{q\to\infty} \lambda = \infty$) as $n^* < 0$ for these values, therefore it does not have to be taken into account. Parameters: $a = 2, \delta = 0.1, \alpha = -0.75, \beta = -0.05$. Also the case with $\alpha = 0.4$ was tested showing that $\omega_2 > \omega_1$ in such scenario, the results are not reported here.

thus $\omega_1$ exist only if $a > 0$.

Instead, substituting $\omega_2 = \frac{2aA-A^2}{4}$ we get:

$$\begin{aligned} A\sqrt{a^2 - 2aA + A^2} &= -2aA + A^2 + aA \\ \sqrt{(a-A)^2} &= -a + A \rightarrow |a - A| = -a + A \end{aligned} \tag{43}$$

Thus the solution exist only if:

$$-a + A > 0 \rightarrow -a + a + \frac{\alpha^2}{4\beta} > 0 \rightarrow \frac{\alpha^2}{4\beta} > 0 \tag{44}$$

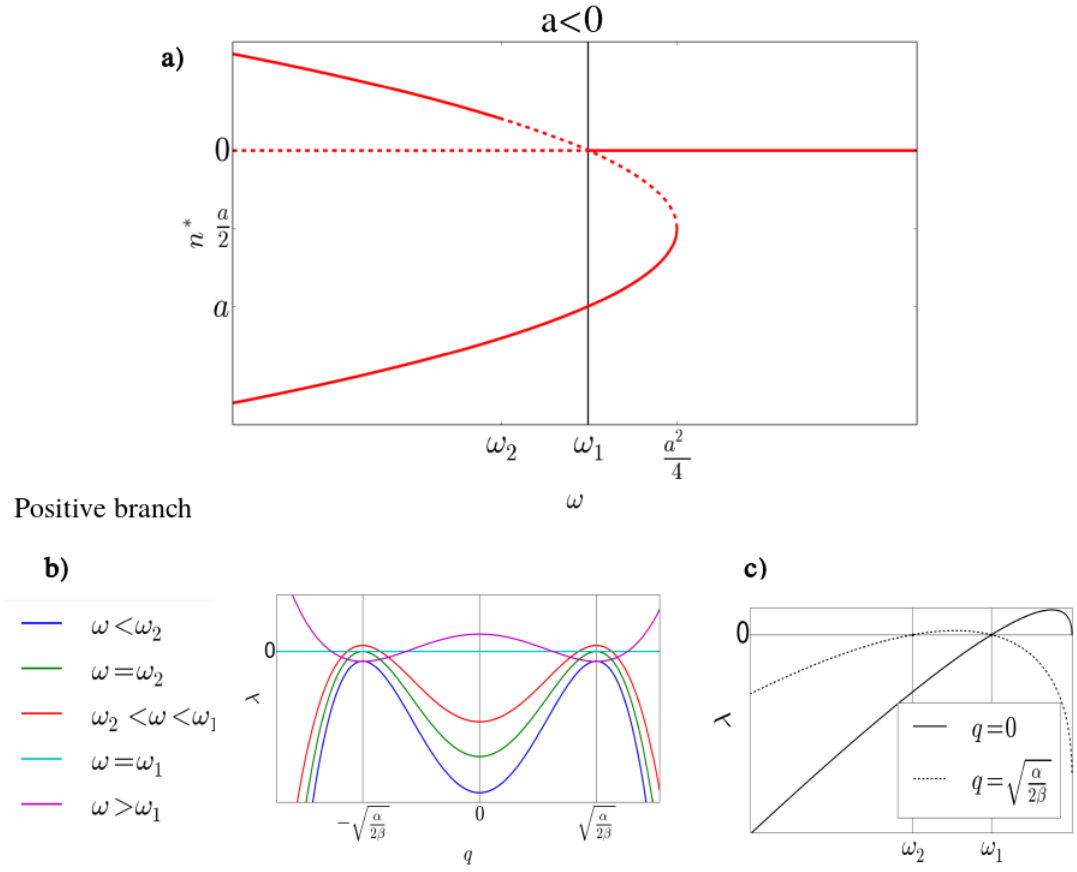


**Figure 5:** The plots sketch the results derived in this section for $a < 0$. a) Represents the bifurcation diagram when introducing the modulation instability point. b) represents the growth rate for different values of $\omega$ for the positive branch ($n^*_+$), as labeled. c) represents the growth rate as a function of $\omega$ for the critical wave numbers. As explained in the text the purple line of b) change the sign ( $\lim_{q\to\infty} \lambda = \infty$) as $n^* < 0$ for these values, therefore it does not have to be taken into account. Parameters: $a = -2, \delta = 0.1, \alpha = -0.75, \beta = -0.05$. Also the case with $\alpha = 0.4$ was tested showing that $\omega_2 > \omega_1$ in such scenario.

which is never verified given $\beta < 0$.

Overall the results are depicted in Fig. 4 and 5. The numerical validation, instead, is reported in Sec. 3.2.

Finally, we plot the dependence of the modulation instability ($MI$) point with the parameter $a$, which, as described in Section 2.1, is the parameter determining the passage from the sub-critical to the supercritical scenario. The results are depicted in Fig. 6 and 7, where we show the colored version delimiting the areas with equal scenario, as described in the caption.

### 2.2.3 Singularity of the model

The results presented in the previous subsections determine that the model studied so far is singular. For example in Fig. 4 $d$ and Fig. 5 $b$, we notice that for $\omega = \omega_1 = 0$ all wave numbers have identical growth rate equal to zero. Indeed, there are two transitions occurring at the same point when $\omega = 0$ (the Turning/Pattern Forming instability occurs on the top of the Transcritical bifurcation for all wave numbers) as represented in Fig. 6. As a matter of fact, there is a high order degeneracy with an infinite number of zero eigenvalues, which overall makes the system structurally unstable.
Furthermore, the model which we are trying to approximate with this equation presents,in the super-critical case, two $\omega$ values corresponding to $MI$ points, for some parameters. In the equation studied

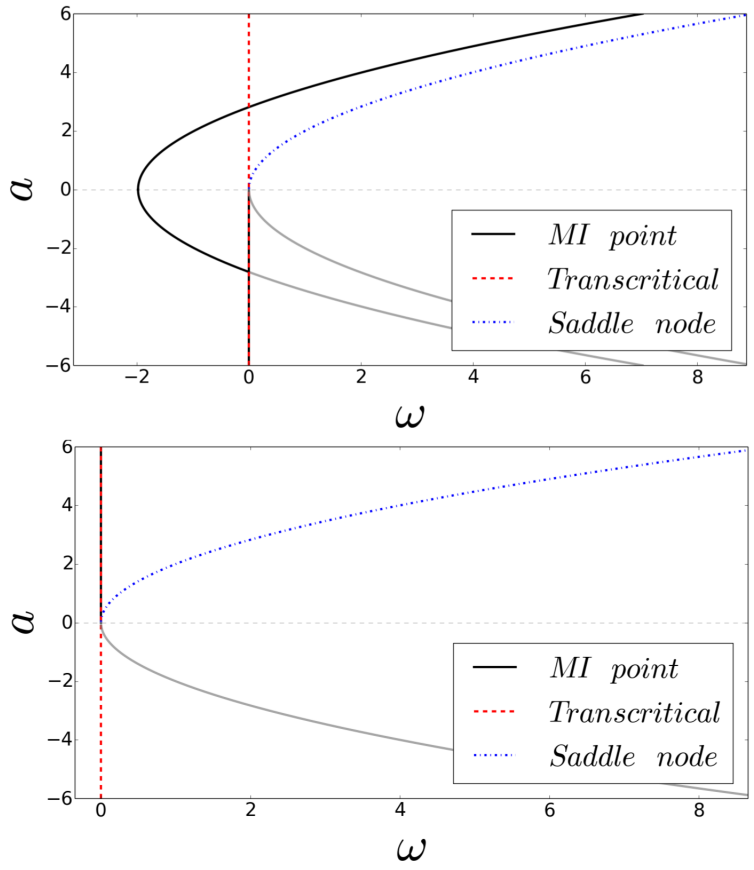


**Figure 6:** In this plot we depict how the modulation instability ($\omega = MI$) points varies with $a$, the parameter which determines the passage from the sub-critical ($a > 0$) to supercritical ($a < 0$) scenario, rather we produce a phase diagram. In the upper picture we consider the positive branch and in the lower picture the negative one. The colored lines depict the $MI$, Transcritical and Saddle point for the different parameters, as labeled. The gray lines depicts the analytical solution in the regions in which $n^* < 0$, which do not make any physical meaning as described in the text, we depict them for clarity of representation. Parameters: $\delta = 0.1$, $\alpha = 0.75$, $\beta = 0.05$

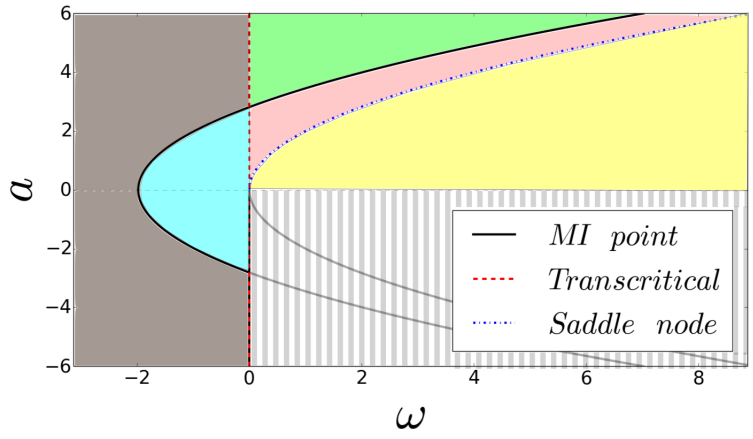


**Figure 7:** In this plot we depict a re-elaborated version of Fig.6 depicting the different areas and fixed points (f.p.): Yellow) 1 f.p. stable $n*_0 = 0$; Pink) 3 f.p.: 2 unstable to Patterns ( $n^*_{+/-} = \frac{a \pm \sqrt{a^2 - 4\omega}}{2}$ ) and 1 stable ($n^*_0 = 0$); Green) 3 f.p.: 2 stable ($n^*_0$ and $n^*_+$) and 1 unstable ($n^*_-$); Blue) 2 f.p.: both unstable ($n^*_0$ and $n^*_+$) to Patterns; Brown) 2 f.p.: 1 stable ($n^*_+$) and 1 unstable ($n^*_0$). Parameters: $\delta = 0.1$, $\alpha = 0.75$, $\beta = 0.05$

so far, this scenario is not present.

Therefore, in order to face both mentioned inconveniences (structural instability and inability to catch

the full behavior) we add a small diffusion term to explore how the scenario changes.
Such term models the combined effect of the growth and branching of the apices, which we initially neglected. As we describe in the next section, this combined effect turns to effectively participate in the dynamics.

### 2.3 Linear stability analysis of the spatial system adding a diffusion

In this section we develop the linear stability analysis of the full equation (Eq. (19)) adding a diffusion term $\epsilon\nabla^2 n$.

$$\partial_t n = -\omega n + an^2 - n^3 + \delta|\nabla n|^2 + \alpha(\nabla^2 n)n + \beta(\nabla^4 n)n + \epsilon\nabla^2 n \tag{45}$$

In this case the growth rate, derived as before, is:

$$\lambda = -\omega + 2an^* - 3n^{*2} - \alpha q^2 n^* + \beta q^4 n^* - \epsilon q^2 \tag{46}$$

As before, we set $\beta < 0$, such that $\lim_{q\to\infty} \lambda = -\infty$, else the system would diverge to $+\infty$ for large $q$. Then we evaluate the first derivative to find the maximum and minimum of $\lambda$, yielding:

$$\frac{\partial\lambda}{\partial q} = -2(\alpha n^* + \epsilon)q + 4\beta q^3 n^* = 2q(-\alpha n^* - \epsilon + 2\beta n^* q^2) = 0 \rightarrow \begin{cases} q_c = 0 \\ q_c = \pm\sqrt{\frac{\alpha n^* + \epsilon}{2\beta n^*}} = \pm\sqrt{\frac{\alpha}{2\beta} + \frac{\epsilon}{2\beta n^*}} \end{cases} \tag{47}$$

We are interested in studying the emergence of patterns, rather we want to study the case in which the fastest growing $q_c \neq 0$. The maximum at $q_c = \sqrt{\frac{\alpha n^* + \epsilon}{2\beta n^*}}$ exist if $\alpha < -\frac{\epsilon}{n^*}$, indeed we require $\beta < 0$, as before, or the growth rate for large wavenumbers would diverge.
Then, we substitute the positive $q_c \neq 0$ to Eq. (46)

$$\begin{aligned} \lambda_c &= -\omega + 2an^* - 3n^{*2} - \alpha n^*(\frac{\alpha}{2\beta} + \frac{\epsilon}{2\beta n^*}) + \beta n^*(\frac{\alpha^2}{4\beta^2} + \frac{\epsilon^2}{4\beta^2 n^{*2}} + \frac{\alpha\epsilon}{2\beta^2 n^*}) - \epsilon(\frac{\alpha}{2\beta} + \frac{\epsilon}{2\beta n^*}) = \\ &= -\omega + 2an^* - 3n^{*2} - \frac{\alpha^2 n^*}{4\beta} - \frac{\epsilon^2}{4\beta n^*} - \frac{\alpha\epsilon}{2\beta} \end{aligned} \tag{48}$$

So:

$$\lambda_c = -\omega + 2an^* - 3n^{*2} - \frac{(\alpha n^* + \epsilon)^2}{4\beta n^*} \tag{49}$$

Solving this equation analytically for $\omega$ after substituting $n^*_+ = \frac{a+\sqrt{a^2-4\omega}}{2}$ and $n^*_- = \frac{a-\sqrt{a^2-4\omega}}{2}$ is not straightforward. In *Appendix A*.1 we further develop the expression until reaching a third order polynomial in $\omega$ where two of its real solutions represent the analytical expression of the $MI$ points. Here, we show the results (confirmed in *Appendix A*.1) obtained by solving (49) with an algorithm to detect the combination of $\omega$ and $a$ which determines that the growth rate is zero. Such combinations are critical values as they determine the passage from positive (pattern forming instability) to negative (stable fixed point) growth rate. In Fig. 8 we report the results for the positive branch, as the negative branch do not give any solution. The gray lines, as in the previous section, represent the evolution when $n < 0$ which do not make any physical meaning, we show them for clarity.

We notice that the region in which 2 MI points coexist do not only depend on $a$ and $\omega$, but also on the other parameters. For the previous case it was possible to determine analytically the effect of each parameter which is less direct in this case. In *Appendix A*.2 we show some other combinations.

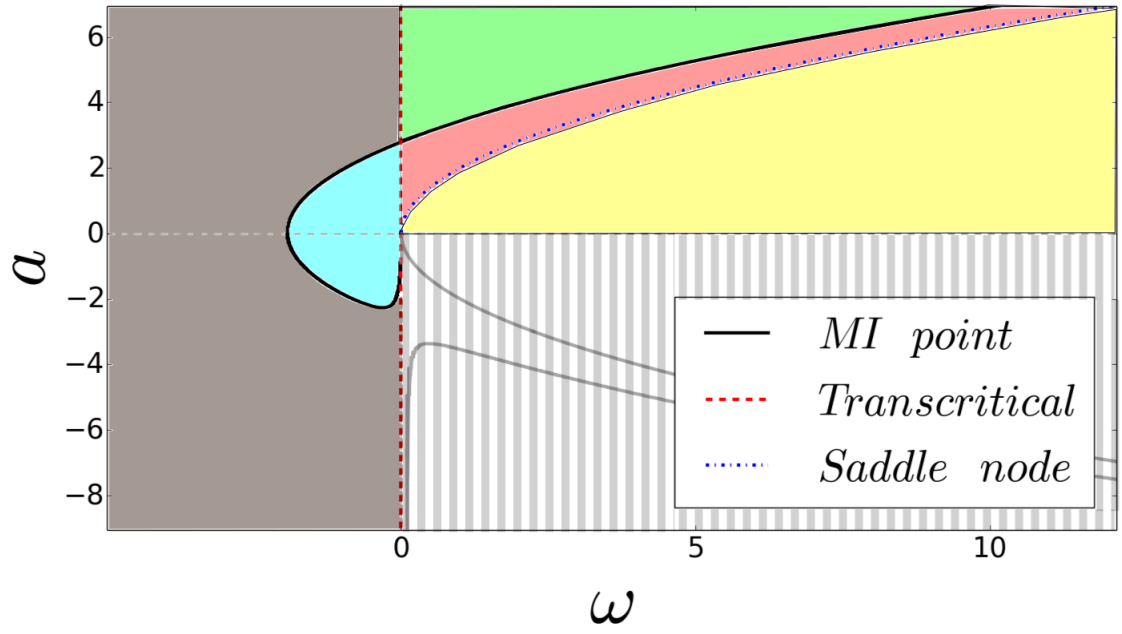


**Figure 8:** In this plot we depict how the modulation instability ($MI$) points varies with $a$, the parameter which determines the passage from the sub-critical ($a > 0$) to supercritical ($a < 0$) obtaining the phase diagram. To obtain this plot we solved numerically Eq. (49) for $n_+^*$. The colored line depict the $MI$, Transcritical and Saddle point for the different parameters, as labeled. The gray lines depict the analytical solutions in the regions in which $n^* < 0$, which do not make any physical meaning, we depict them for clarity of representation. Further we depict as before the different areas and fixed points (f.p.): Yellow) 1 f.p. stable $n*_0 = 0$; Pink) 3 f.p.: 2 unstable to patterns ( $n_{+/-}^* = \frac{a \pm \sqrt{a^2 - 4\omega}}{2}$ ) and 1 stable ($n_0^* = 0$); Green) 3 f.p.: 2 stable ($n_0^*$ and $n_+^*$) and 1 unstable ($n_-^*$); Blue) 2 f.p.: both unstable to patterns ($n_0^*$ and $n_+^*$); Brown) 2 f.p.: 1 stable ($n_+^*$) and 1 unstable ($n_0^*$). Parameters: $\delta = 0.1$, $\alpha = 0.75$, $\beta = 0.05$, $\epsilon = 0.005$

Overall we confirm that this scenario reproduce exactly the case observed in the full $ABD$ model (Ruiz et al., 2016).

# 3 Numerical validation

In this section we numerically validate:

- the hypothesis made in Sec. 1.2 on the term $\delta|\nabla n(x,y,t)|^2$;
- the analytical results derived in Sec. 2;
- that the phase diagram including the region of stability of the different patterns of Eq. (19) is analogous to the one obtained in the $ABD$ model (Ruiz et al., 2016).

In order to simulate the partial differential equation we considered periodic boundary conditions and used a Pseudospectral method. The idea behind such method is the separation between linear and non linear term of the PDE (Toral and Colet, 2014). In our case the linear part is :

$$\mathcal{L}[n] = -\omega n \tag{50}$$

and the non linear is:

$$\mathcal{N}[n] = an^2 + bn^3 + \delta|\nabla n|^2 + \alpha(\nabla^2 n)n + \beta(\nabla^4 n)n \ . \tag{51}$$

The linear term is evaluated directly in Fourier space, instead the non linear one is evaluated in real space and than transformed back.
In particular we used the so-called two-step (or mid-point) method, following (Montagne et al., 1997). We performed the simulations without considering the small diffusion, which else would introduce in the linear part the following term:

$$\mathcal{L}[n] = -\omega n + \epsilon\nabla^2 n \tag{52}$$

However, we expect that all results we are presenting would be equal if considering the small diffusion given that we test a range of parameters in which the phase diagrams are equal (notice that for $a > 0$ Fig. 7 and Fig. 8 are equal).

## 3.1 Confirming the effect of $\delta|\nabla n(x,y,t)|^2$

As described in the introduction, we are trying to reproduce with this equation the behavior emerging from the multidimensional model described in (Ruiz et al., 2016). In such model the growth velocity of the front have two features:

- It seems to be mainly based on the growth of the apices, perpendicular to the fronts.
- When starting from random initial patch without radial symmetry the system evolves to a circular domain.

We modeled these features through the term $\delta|\nabla n(x,y,t)|^2$ derived as described in Sec. 1.2. Here, we numerically validate that $\delta|\nabla n(x,y,t)|^2$ reproduce the features exposed above.

**Reducing the equation.** For such purpose we study Eq. (19) considering $\beta = 0$:

$$\partial_t n = -\omega n + an^2 - n^3 + \delta|\nabla n|^2 + \alpha(\nabla^2 n)n \tag{53}$$

In this way we can focus on the effect of $\delta|\nabla n|^2$. Instead, we can not consider $\alpha = 0$ as the term is needed to stabilize the system in particular to damp the large wavenumbers, (in particular with $\alpha > 0$ the system is stable), indeed it enables to maintain the steepens of the front constant, which otherwise would cause numerical problems.

### 3.1.1 Exploring the dependence of $\delta$ with the velocity of expansion.

In this section we show the results of running the simulation for different values of $\delta$ and evaluating the relative velocity of growth when starting from different initial conditions (spot or stripe of plants). Further we changed also the other parameters in order to include or rule out the possibility of a dependence.

As shown in Fig. 9 we confirm that the velocity of growth depends linearly with $\delta$, which models the growth of the apices, however we also see a dependence with the death-life rate $\omega$ and the coefficient $a$. We explore in detail the dependence on these other parameters in *Appendix B*.

Further, we confirm that the growth velocity of a stripe initial condition is faster than the one of a circular domain for equal $\delta$. Such effect is given by the curvature of the front which introduce an additional negative force to overcome for the populated solution when expanding over the unpopulated one (Gomila et al., 2001).

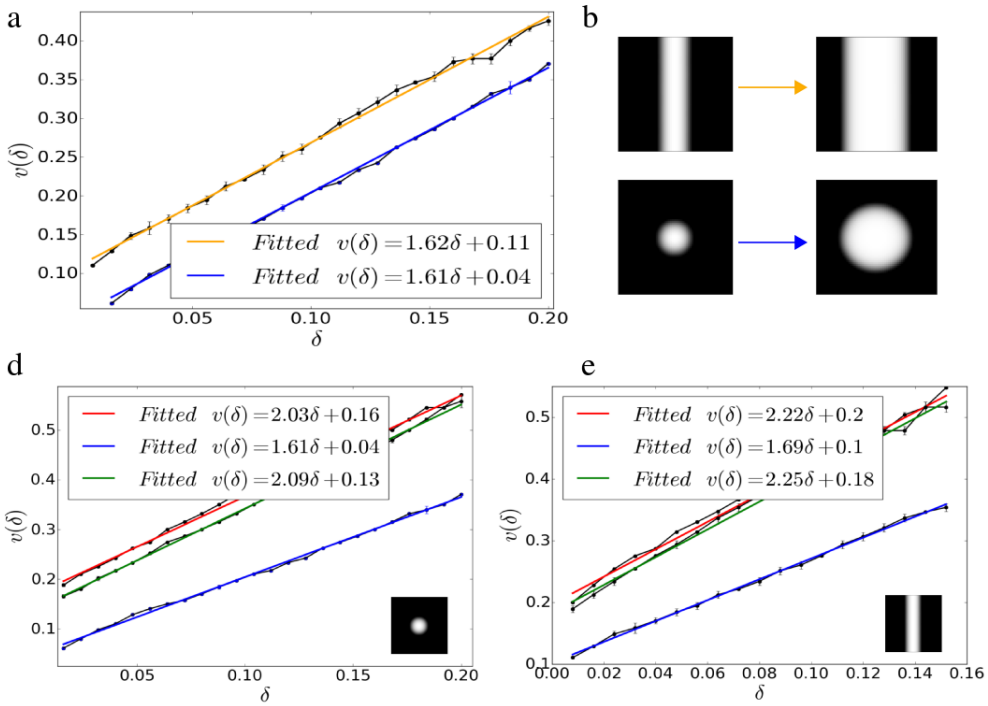


**Figure 9:** The plot shows the dependence of the growth velocity with $\delta$. In a) we compare the velocity for circular (*blue*) and stripe (*orange*) initial conditions (Parameters: $\omega = 0.6, a = 2$). In b) we show an example of the growth for both initial conditions, the times of the snaps are $t = 0$ (left), $t = 40$ (stripe,right), $t = 80$ (circle,right). In d) and e), we show the dependence of the velocity with the other parameters. (Parameters: Green lines: $\omega = 0.6, a = 2.2$; Red lines: $\omega = 0.4, a = 2$; Blue lines: $\omega = 0.6, a = 2$). The plotted velocity is the average over 2 directions of growth, orientated between each others in a perpendicular (for the circular initial condition) and anti-parallel(for the stripe initial condition) way. All directions of growth are considered perpendicular to the front. The bars represent the standard deviation of the average. Parameters equal in all plots: $\alpha = 0.5$, $\Delta x = \Delta y = 0.3$, $\Delta t = 10^{-4}$.

### 3.1.2 Growth dynamics with random initial condition lacking of radial symmetry

In this section we show that if the starting initial domain is a random patch lacking of radial symmetry, the dynamical evolution of Eq. (53) tends to reduce the curvature differences firstly leading to a circular domain which then keeps expanding.
Such result on one side reproduces the effect noticed in the $ABD$ model, thus validating Eq. (19) as a good approximation. On the other side it validates the analytical results already studied in (Gomila et al., 2001), where the authors formalize such effect for a prototypical model of spatial system.
In Fig. 10 we report an example.

**Figure 10:** In this plot we show the evolution of Eq. (53) for an arbitrary shaped domain at $t = 1, 5, 10, 15, 20$ from left to right. Parameters: $\omega = 0.5$, $a = 2, \delta = 0.1, \alpha = 0.5, \beta = 0$, $\Delta x = \Delta y = 0.3$, $\Delta t = 10^{-3}$.

### 3.2 Bifurcation diagram including stability regions of patterns

In this section we show the numerical validation of the analytical results derived in Sec. 2.2 as well as the analogy between the bifurcation diagram of Eq. (19) and the one of the $ABD$ model. In particular, on one side we verify that the precise position of the $MI$ point coincide with the one derived, and on the other side we study the region of existence of the different patterns. To obtain this latter result we started the simulations with the pattern as an initial condition and verified for which $\omega$ values each of them is maintained.

As shown in the results depicted in Fig. 11 we confirm that the bifurcation diagram is analogous to the one obtained in the $ABD$ model.

**Studied scenario:** The results were taken integrating Eq. (19) and considering the sub-critical system ($a > 0$). In such scenario the addition of diffusion leave the phenomenology invariant (in the parameter range that we are considering the $a - MI$ curve is such as Fig. 8, rather for all $\omega$ the behavior is the same as without diffusion).

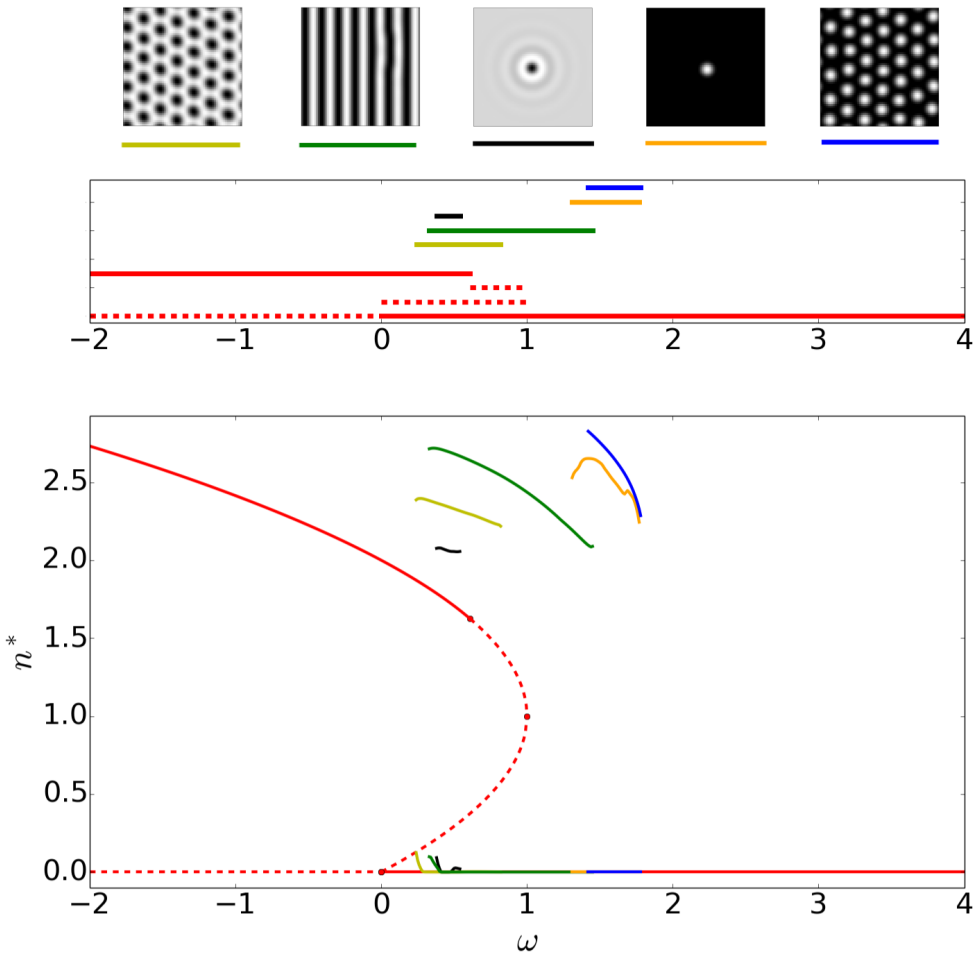


**Figure 11:** The plot depicts the stability of the four patterns depicted in the figures above when initializing the system with each specific pattern, thus yielding the bifurcation diagram. From left to right negative hexagons (light green), stripes (green), negative soliton (black), positive soliton (orange), positive hexagons (blue). Further the homogeneous populated and unpopulated solution is depicted in red. In the upper plot it is depicted the region of existence only in $\omega$, to simplify visualization. In the lower picture the maximum and the minimum value of the density $n$ is depicted. Parameters: $a = 2, \delta = 0.1, \alpha = -0.5, \beta = -0.05$, $\Delta x = \Delta y = 0.3$, $\Delta t = 10^{-4}$.

## 4 Re-population strategies

Given the results presented in the previous section, which confirmed that we can approximate the $ABD$ model with Eq. (45), we used the equation to get general results over clonal plants growth.
In particular we explored numerically the possibility of re-population strategies when considering the system in a scenario in which the sole fixed point of the homogeneous solutions is $n^* = 0$ (occurs for $\omega > \frac{a^2}{4}$, Sec. 2.1) coexisting with positive hexagons, positive solitons and stripes.
We considered as initial condition having a fixed number of plants and explored if it exist an optimal density of how to plant the initial circular patch to promote growing and avoid extinction.
The results, depicted in Fig. 12, confirm that it exists an optimal density. For example we see that the first left point corresponds to 40 plants planted in a radius of 3 giving a total density of the patch $d = \frac{N}{\pi r^2} = \frac{40}{\pi 3^2} = 1.41$. Such initial condition give rise to a positive soliton, as described in the labels on the right. We notice that having a larger number of plants distributed on a larger circle may give rise to other patterns which include separated solitons. If, for example, we have an original amount of 400 plants than the most efficient way of planting them would be in 10 isolated groups of 40 plants, each distributed in a spot with radius 3 or 4. Indeed the maximum efficiency that we can get by planting the 400 plants all together would be 4 isolated spots (as shown in the graph below the richest pattern that 400 plant can generate if planted together is the red one), instead, by planting them separately, 10 isolated spots could grow simultaneously.

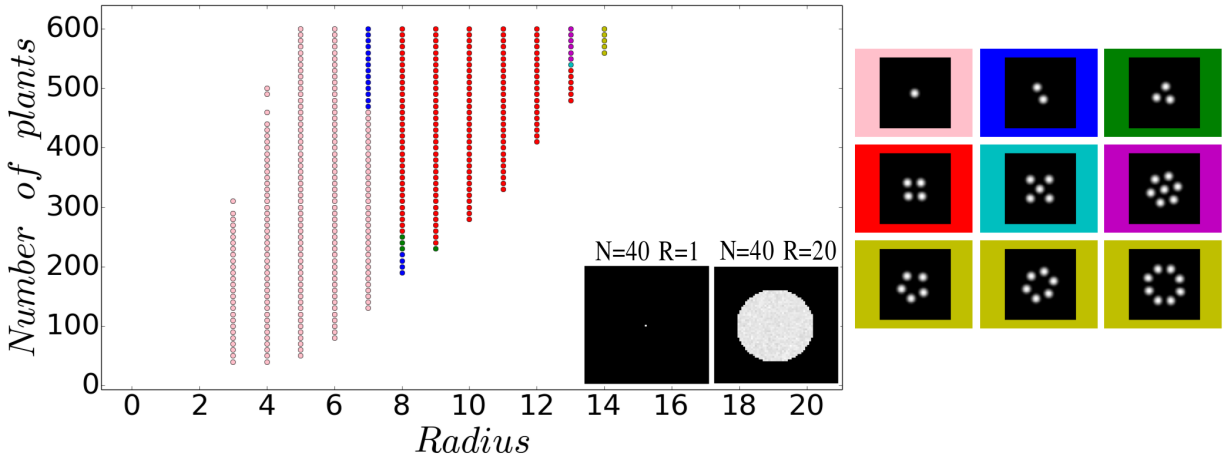


**Figure 12:** In this picture we plot the densities at which a fixed number of plants should be planted to grow. Where no points are present the initial condition is not stable and the evolution converges to no plants. In the inset we show two examples of initial condition for $N = 40$ plants and $radius = 1, 20$ (below the inset there are no points). On the right we show the patterns to which converged the initial circular patch of plants for the different parameters, the color of the frame labels the colors in the plot. The parameters we used correspond to the region in which the only fixed point is $n_0^* = 0$, but where also stripes, positive solitons and hexagons can be stable if inserted as initial condition (Fig. 3). Parameters: $\omega = 1.43$,$a = 2$,$\delta = 0.1$,$\alpha = -0.5$,$\beta = 0.05$, $\Delta x = \Delta y = 0.3$, $\Delta t = 10^{-5}t$, $T_{end} = 100t$.

# 5 Discussion

In this thesis we reproduce the dynamical behavior of a complex numerical model describing the evolution of seagrass meadows (formed by nine two dimensional fields) with a single, analytically tractable, partial differential equation. Furthermore, we use such equation to propose a possible design of re-repopulation strategy. We view this work as a contribution to a larger working frame, attempting to define a comprehensive description of the dynamical features influencing seagrass growth, development and death.

Seagrasses are essential factors in the marine ecosystem as well as efficient carbon sinks needed to limit greenhouse emissions. Despite their relevance, an on-going loss has been occurring since the last mid-century due to anthropogenic factors inducing the deterioration of water quality in the coastal touristic zones (Marbà et al., 2014) as well as the increment of global temperatures (Jordà et al., 2012). For these reasons, we urge to understand how segrasses respond to disturbances in order to predict the effects and limit their loss. On one side, the multiple factors influencing seagrass mortality is reasonably well investigated and an increasing amount of studies are leading toward accurate numerical models reproducing real measurements. However little is still known about analytical models providing a global description of the dynamical features of seagrasses.

Inspired by previous works providing an accurate numerical model ($ABD$ model) of seagrass meadows development and interaction (Ruiz et al., 2016), we used their results to build a partial differential equation reproducing the same behavior. Such formalization would contribute to determine the critical dynamical factors in the loss of seagrasses and to design effective ways to limit their extinction.

**Overview of the results:** In the presented thesis we show that a single partial differential equation can reproduce the dynamical features of the $ABD$ model (Ruiz et al., 2016).

In Sec. 1.2 we describe how we derived the equation and the assumptions we took. In Sec. 2.1 we perform the linear stability analysis of the homogeneous system showing that it reproduces the basic bifurcation diagram (transcritical bifurcation and saddle node) of the numerical model, then we expand the analysis introducing the spacial derivatives in Sec. 2.2 thus determining the modulation instability points. Such study lead us to the conclusion that an additional factor was missing to the original formulation, as exposed in Sec. 2.2.3. Thus in Sec. 2.3 we repeat the analysis including the new term and see that the equation reproduces exactly the dynamical results of the $ABD$ model. Starting from Sec. 3 we perform numerical validations, firstly we show that the terms we inserted reproduce the expected features (Sec. 3.1) then we verify that the regions of pattern formation are in accordance with the analytical results (Sec. 3.2 ). Finally we use the model to show the potentiality in designing effective re-population strategies for seagrasses (Sec. 4).

**Future perspectives:** The overall goal of this research direction is to provide a comprehensive description of the dynamical evolution of clonal plants.

A follow up of this thesis, therefore, would include defining the accurate relation between the parameters of the simplified PDE that we derived with real measurements. Such objective could be addressed by a backward approach: Firstly we could study the exact relation with the parameters of the $ABD$ model, then, as already introduce in (Ruiz et al., 2016), we could relate those with the once in the precedent model (Sintes et al., 2005), which are directly comparable with specie-specific real parameters.

On one side this would give us a clue over the boundaries of our approach in catching detailed bio-

logical features but, on the other side, it would provide the exact contribution of macro biological features in the dynamical properties emerging from meadows of seagrass.
Once gained such a control our approach could be used for different purposes. For example it could be applied as a tool to focus the investigation in biology on one or the other feature of seagrasses or, as already proposed in Sec. 4, it could be adopted to design time and resource efficient re-population strategies.

# 6 Appendix A: Further studies on the model in Sec. 2.3

In this appendix we show further analysis on the model presented in Sec. 2.3.

## 6.1 A.1: Analytical solutions of the model

Here we start from Eq. 49 in order to find the roots in $\omega$.
We set the equation to zero and re-elaborate as follows:

$$\begin{aligned}\lambda_c &= -\omega + 2an^* - 3n^{*2} - \frac{(\alpha n^* + \epsilon)^2}{4\beta n^*} = 0 \\ (4\beta n^*)(-\omega + 2an^* - 3n^{*2}) &- \alpha^2 n^{*2} - \epsilon^2 - 2\alpha n^* \epsilon = 0\end{aligned} \tag{54}$$

Thus we substitute the positive fix point $n^*_+ = \frac{a+\sqrt{a^2-4\omega}}{2}$, yielding:

$$\begin{aligned}&(\beta a + \beta\sqrt{a^2-4\omega})(4\omega - a^2 - a\sqrt{a^2-4\omega}) - \frac{\alpha^2}{2}(a^2 - 2\omega + a\sqrt{a^2-4\omega}) - \epsilon^2 - \alpha\epsilon(a + \sqrt{a^2-4\omega}) = 0 \\ &2\beta a(4\omega - a^2) + \sqrt{a^2-4\omega}(2\beta)(2\omega - a^2) - \Big(\frac{\alpha^2}{2}(a^2-2\omega) + \epsilon^2 + \alpha\epsilon a\Big) - \sqrt{a^2-4\omega}\Big(\frac{a\alpha^2}{2} + \alpha\epsilon\Big) = 0\end{aligned} \tag{55}$$

So we rearrange and get:

$$\sqrt{a^2-4\omega}\Big(4\beta\omega - 2\beta a^2 - \frac{a\alpha^2}{2} - \alpha\epsilon\Big) = (-8\beta a - \alpha)\omega + 2\beta a^3 + \epsilon^2 + \alpha\epsilon a + \frac{\alpha^2 a^2}{2} \tag{56}$$

To simplify we define the variables $A \equiv -2\beta a^2 - \frac{a\alpha^2}{2} - \alpha\epsilon$, $B \equiv 4\beta$, $C \equiv +2\beta a^3 + \epsilon^2 + \alpha\epsilon a + \frac{\alpha^2 a^2}{2}$ and $D \equiv -8\beta a - \alpha^2$. Thus:

$$\sqrt{a^2-4\omega} = \frac{C + D\omega}{A + B\omega} \tag{57}$$

Squaring both sides and re-arranging we obtain:

$$(4B^2)\omega^3 + (-B^2a^2 + 8AB + D^2)\omega^2 + (-2ABa^2 + 4A^2 + 2CD)\omega - Aa^2 + C^2 = 0 \tag{58}$$

Substituting back the previous variables we obtain:

$$\mathcal{A}\omega^3 + \mathcal{B}\omega^2 + \mathcal{C}\omega + \mathcal{D} = 0 \text{ with } \begin{cases}\mathcal{A} = 64\beta^2 \\ \mathcal{B} = \alpha^4 - 16a^2\beta^2 - 32\epsilon\alpha\beta \\ \mathcal{C} = 2\alpha^2\epsilon^2 + 2\alpha^3\epsilon a + 8a^2\beta\alpha\epsilon - 16a\beta\epsilon^2 \\ \mathcal{D} = 4\epsilon^2 a^3\beta + \epsilon^2\alpha^2 a^2 + 2\epsilon^3\alpha a + \epsilon^4\end{cases} \tag{59}$$

We did not elaborate further the derivation, but, by solving numerically the cubic polinomial we verified that two of the real solutions of Eq. (59) are the solutions of the system evaluated by solving numerically Eq. (49), instead the third solution is artificial and generated when squarig both sides of the equations. In Fig. 13 we report the results.

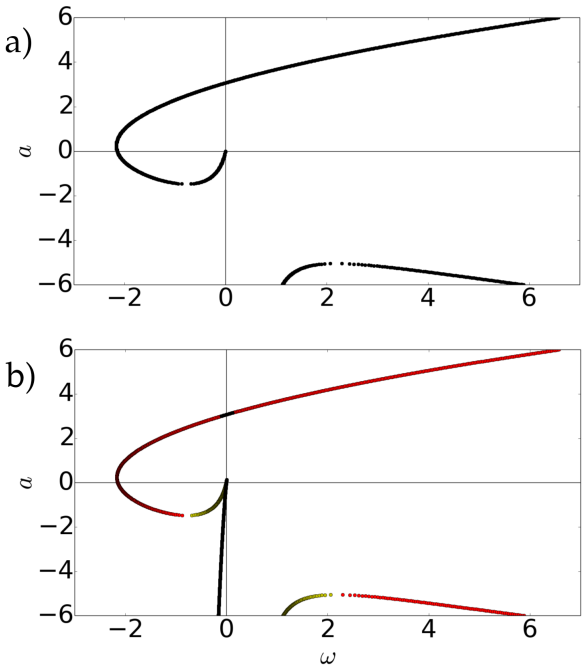


**Figure 13:** In this plot we compare the results derived when solving numerically a) Eq. (49) and b) Eq. (59). In this case the three real solutions are depicted with different colors. We see that one of the solutions is not present in the real system as it is artificially generated when squaring. Parameters: $\delta = 0.1$,$\alpha = 0.8$,$\beta = -0.05$, $\epsilon = 0.005$

## 6.2 A.2: Phase diagram with different parameters

In this appendix we show that with larger $\epsilon$ and changing $\alpha$ the region in which two modulation instability points exist varies. For example it can exist in the subcritical case as well. In Fig. 14 we show the results.

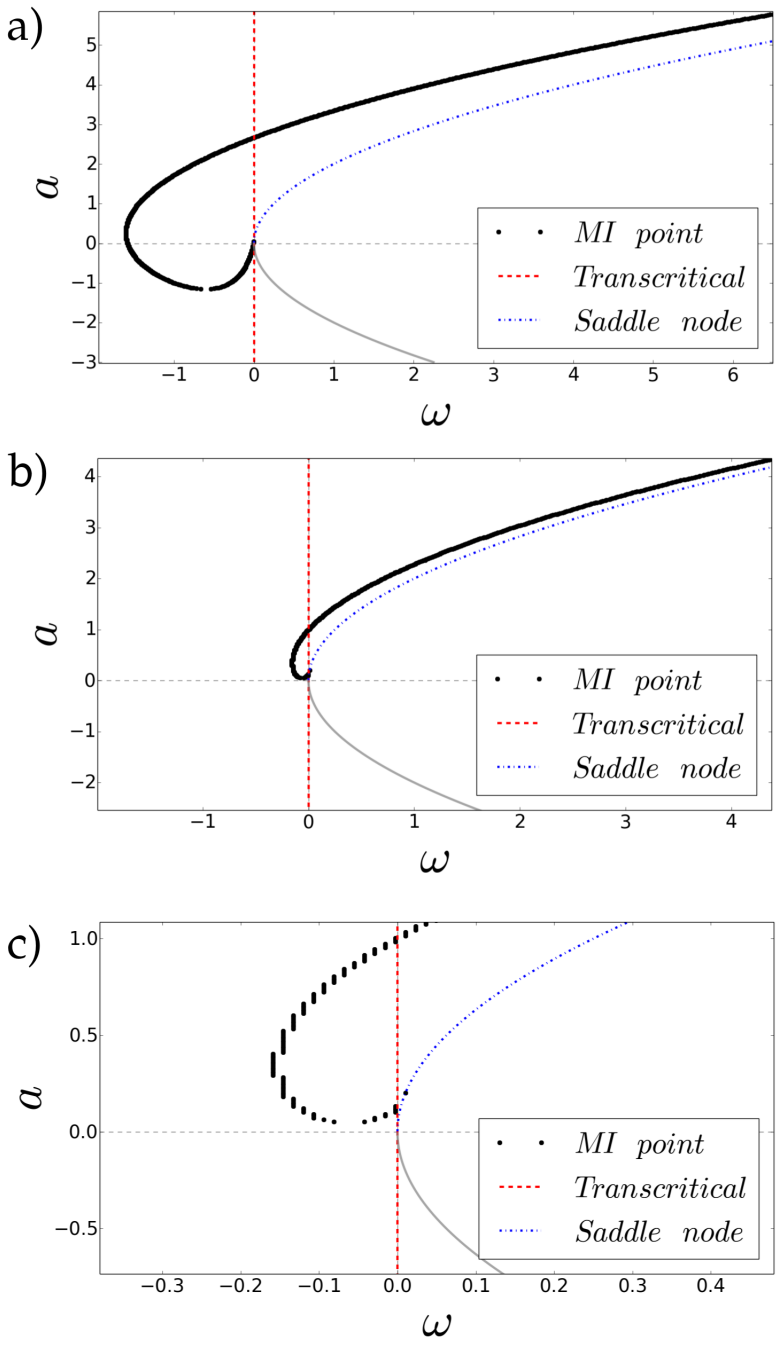


**Figure 14:** In this plot we show that certain combinations of the parameters change the $a, \omega$ region where two $MI$ points exist. In a) $\alpha = 0.75$, in b)$\alpha = 0.5$. In c) we show a zoom in of the plot b) to visualize that the modulation instability point ends on the saddle node. Parameters : $\delta = 0.1$, $\beta = -0.05$, $\epsilon = 0.05$

# 7 Appendix B: Influence of the parameters $a$, $\omega$ and $\alpha$ on the growth velocity

In this appendix we analyze numerically Eq. (53). In particular we focus on the relation between the growth velocity and the parameters $a$, $\omega$ and $\alpha$, given the apparent dependence presented in Section 3.1.1. Indeed, we noticed that the velocity at which the front grows do not depend only on $\delta$ but seems to have a non negligible contribution from the other parameters as well.

For all the following results we consider stripes of plants as an initial condition to avoid introducing the curvature effects mentioned in Section 3.1.1.

We tested systemically the dependence of the growth velocity on $a$, $\omega$ and $\alpha$. The results, depicted in Fig.15, show that there is a clear dependence on $a$ and $\omega$, instead $\alpha$ does not vary the velocity (results not shown). In particular we used values of $a > 4\omega$ for the first plot and values of $\omega < a^2/4$ for the second, in order to limit in the parameter region where the homogeneous solutions exist.

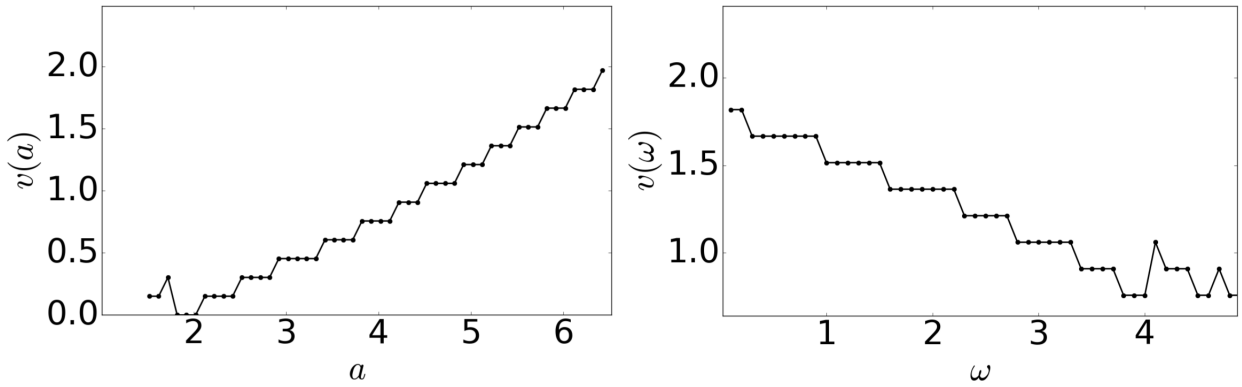


**Figure 15:** The plot depicts the dependence of the growth velocity with $a$ and $\omega$, as labeled. In the plot on the left $\omega = 0.5$, in the plot on the right $a = 5$. Parameters equal in all plots: $\delta = \alpha = 0.5$, $\Delta x = \Delta y = 0.3$, $\Delta t = 10^{-3}$

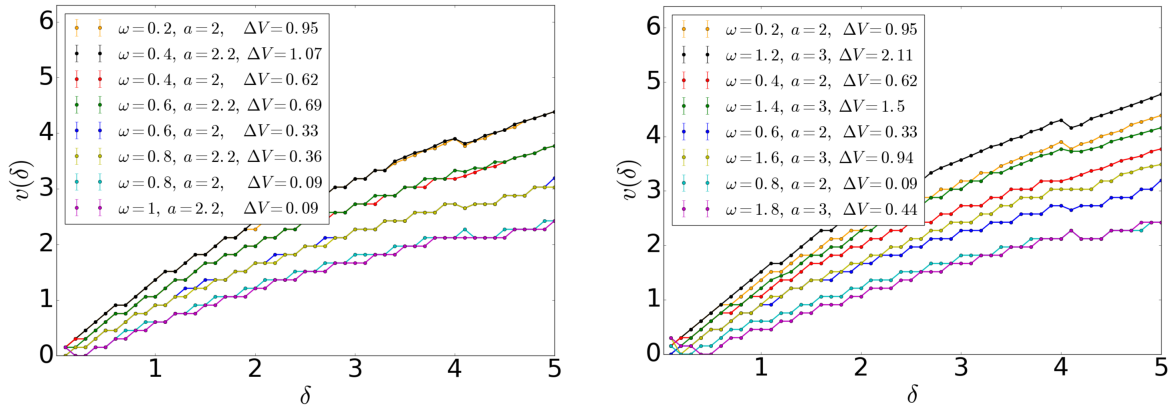


**Figure 16:** The plot depicts the dependence of the growth velocity with $\delta$, $a$ and $\omega$ as reported in the label, comparing with the difference in potential. We get contradictory results. For small values of $a$ and $\omega$ the difference in potential (Eq. (60)) seems to approximate well the difference in velocity (left panel). For larger values, instead, it is not (right panel) . Parameters equal in all plots: $\alpha = 0.5$, $\Delta x = \Delta y = 0.3$, $\Delta t = 10^{-3}$

**Lyapunov function** We attempted to explain why $a$ and $\omega$ contributes to the velocity quantifying the tendency to move of the front. For this purpose we evaluated the Lyapunov function between the homogeneous and the null solutions, thus determining the potential difference. We hypothesized that the higher the potential difference the faster the velocity of growth.
A Lyapunov function is defined as $V(n) \geq C$, being $C$ a constant, and $\frac{dV(n)}{dt} < 0$. If we neglect the derivative terms, a function satifying the exposed requisites is:

$$\Delta V(n) = -\int_{n=0}^{n^*} \dot{n}(t)\partial n = -\int_{n=0}^{n^*} (-\omega n + an^2 - n^3)\partial n = -\Big(-\frac{\omega n^{*2}}{2} + \frac{an^{*3}}{3} - \frac{n^{*4}}{4}\Big) \tag{60}$$

with $\Delta V(n) = V(n) - V(0)$. Substituting the fixed point $n_+^* = \frac{a+\sqrt{a^2-4\omega}}{2}$ found in (21), we get:

$$\Delta V(n) = \frac{a^4}{24} - \frac{a^2\omega}{4} - \frac{1}{6}a\omega\sqrt{a^2-4\omega} + \frac{1}{24}a^3\sqrt{a^2-4\omega} + \frac{\omega^2}{4} \tag{61}$$

We tested different combinations of $a$ and $\omega$, and got contradictory results. If on one side for small values of $a$ and $\omega$ we verified that the higher the velocity the higher the potential (Fig. 16 left) on the other side when increasing the values the velocity is not consistent with the prediction. In reality the dependence seems to be around a value close to $a - \omega$ (Fig. 16).
Overall, we do not provide an analytical explanation of why the velocity depends on $a$ and $\omega$.
Evaluating the potential as in Eq. (60), thus neglecting the factors $\delta|\nabla n|^2 + \alpha(\nabla^2 n)n$ may be the cause of the problem, as it is probably not a good approximation. Further analysis are needed to explain the phenomena.
We will not focus here on such issue as the main purpose of the thesis is reproducing the behavior of the $ABD$ model, which we do reproduce.

## References


Daniel Ruiz, Damià Gomila, Tomás Sintes, Emilio Hernández-García, Núria Marbà, and Carlos M. Duarte. Fairy circles under the sea, 2016. *Preprint*.

Carlos M Duarte and Carina L Chiscano. Seagrass biomass and production: a reassessment. *Aquatic botany*, 65(1):159–174, 1999.

Carlos M Duarte. The future of seagrass meadows. *Environmental conservation*, 29(02):192–206, 2002.

James W Fourqurean, Carlos M Duarte, Hilary Kennedy, Núria Marbà, Marianne Holmer, Miguel Angel Mateo, Eugenia T Apostolaki, Gary A Kendrick, Dorte Krause-Jensen, Karen J McGlathery, et al. Seagrass ecosystems as a globally significant carbon stock. *Nature Geoscience*, 5(7):505–509, 2012.

Elizabeth Mcleod, Gail L Chmura, Steven Bouillon, Rodney Salm, Mats Björk, Carlos M Duarte, Catherine E Lovelock, William H Schlesinger, and Brian R Silliman. A blueprint for blue carbon: toward an improved understanding of the role of vegetated coastal habitats in sequestering co2. *Frontiers in Ecology and the Environment*, 9(10):552–560, 2011.

Gabriel Jordà, Núria Marbà, and Carlos M Duarte. Mediterranean seagrass vulnerable to regional climate warming. *Nature Climate Change*, 2(11):821–824, 2012.

Núria Marbà, Elena Díaz-Almela, and Carlos M Duarte. Mediterranean seagrass (posidonia oceanica) loss between 1842 and 2009. *Biological Conservation*, 176:183–190, 2014.

R.D. Routledge. Spatial patterns arising from plant dispersal as modelled by a correlated random walk. *Journal of Applied Probability*, 27(1):1–13, 1990.

Tomas Sintes, Núria Marbà, Carlos M Duarte, and Gary A Kendrick. Nonlinear processes in seagrass colonisation explained by simple clonal growth rules. *Oikos*, 108(1):165–175, 2005.

James D Murray. *Mathematical biology I: an introduction, Vol. 17 of interdisciplinary applied mathematics*. Springer, 2002.

Damià Gomila. Dynamics of spatial structures in nonlinear optics. 2003.

Raúl Toral and Pere Colet. *Stochastic numerical methods: an introduction for students and scientists*. John Wiley & Sons, 2014.

Raúl Montagne, Emilio Hernández-García, A Amengual, and Maxi San Miguel. Wound-up phase turbulence in the complex Ginzburg-Landau equation. *Physical Review E*, 56(1):151, 1997.

Damià Gomila, Pere Colet, Gian-Luca Oppo, and Maxi San Miguel. Stable droplets and growth laws close to the modulational instability of a domain wall. *Physical Review Letters*, 87(19):194101, 2001.